Article

Optimization of the Ablative Laser Cutting of Shadow Mask for Organic FET Electrode Fabrication

Mariusz Tomczyk [1,*], Paweł Kubik [2] and Witold Waliszewski [2]

[1] Institute of Electrical Engineering Systems, Faculty of Electrical Engineering,
  Electronics, Computer and Control Engineering, Lodz University of Technology, 116, 90-924 Łódź, Poland
[2] Department of Molecular Physics, Faculty of Chemistry, Lodz University of Technology, 116,
  90-924 Łódź, Poland; pawel.kubik@dokt.p.lodz.pl (P.K.); witold.waliszewski@dokt.p.lodz.pl (W.W.)
[*] Correspondence: martom@matel.p.lodz.pl

check for updates

Abstract: This article presents an ablative method of cutting masks from ultra-thin metal foils using nanosecond laser pulses. As a source of laser radiation, a pulsed fiber laser with a wavelength of 1062 nm with the duration of pulses from 15 to 220 nanoseconds (ns), was used in the research. The masks were made of stainless-steel foil with thicknesses of 30 μm, 35 μm, and 120 μm. Channels of different lengths from 50 to 300 μm were tested. The possibilities and limitations of the presented method are described. The optimization of the cutting process parameters was performed using the experiment planning techniques. A static, determined complete two-level plan (SP/DC 2^4) was used. On the basis of the analysis of the test structures, we designed and produced precise shading masks used in the process of organic field effect transistor (OFET) electrode evaporation. The ablative method proved suitable to produce masks with canals of minimum lengths of 70 μm. It offers facile, fast, and economically viable shadow mask fabrication for organic electronics applications, which moreover might enable fast prototyping and circuit design.

Keywords: nanosecond laser ablation; shadow masks fabrication; OFET electrodes deposition; design of the experiment

1. Introduction

Laser technologies are widely used in many industries. For many years, lasers have been successfully used to cut materials such as metals, semiconductors, plastics, and ceramics [1]. The technique of cutting metals with melting and gas blowing is used at a macroscopic scale (the elements of dimensions from 1 to 250 mm) [2]. In the case of cutting precise elements in thin films (30–150 μm), the ablative technique can be used [3]. This method is based on repeated beam scanning along the cut edge and gradual removal of the material. The process has to be repeated many times, depending on the parameters of the laser beam and the thickness of the material. During a single beam scan, a material layer with a thickness of 1 to 5 μm is removed. The ablation method with nanosecond pulses has been successfully used for cutting out unusual shapes of photovoltaic cells [4], surface treatment of silicon and ceramics [5,6], or texturing of rubber surfaces [7]. Laser technologies can also be used in the production of thin-film meta-material structures [8–10]. In this article, we demonstrate the effectiveness of the ablative effect of ns pulses to cut out ultra-thin masks. The created masks have already found application in the production of textronics as well as the electronics elements and systems [11]. One such example is shadow masks used to fabricate electrodes in vapor deposition process of metals. Electrodes prepared by this method are the most mainstream in organic field effect transistors (OFETs) and other organic electronic devices [12,13].

In the last few decades, the evolution from rigid and thick silicone-based electronics to extremely lightweight, thin, and flexible organic electronics has opened the doorway towards next-generation electronic products such as flexible displays, lighting devices, and medical sensors [13–15]. Thanks to the development of flexible OFETs, which are based on organic semiconductors (OSCs), it is possible to fabricate highly flexible electronic systems. A transistor is an electronic component based on semiconductors, which serves as switch and is essential in any electronic circuits [16,17]. One of the promising applications of OFETs are the flexible devices, which can be fabricated by alternating deposition of thin layers of OSC, metal electrodes, and polymer insulator (Figure 1) [17,18].
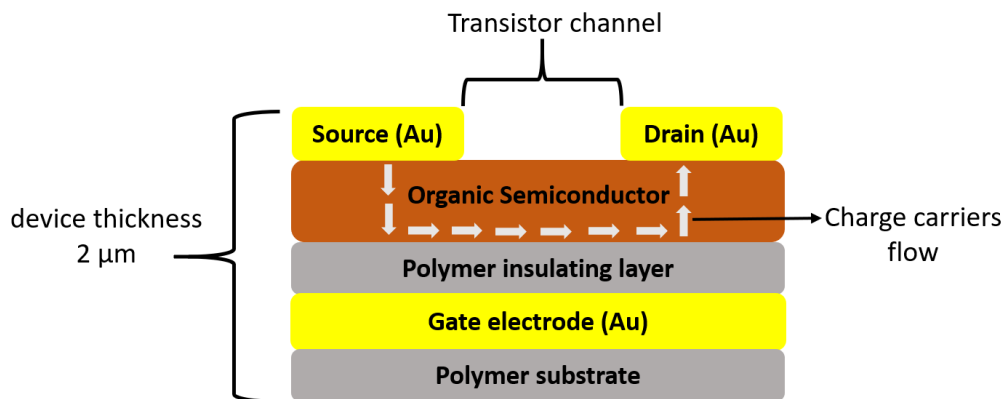

Figure 1. Scheme of flexible organic transistor in bottom gate–top contact electrode configuration.

The transport of charge carriers occurs through active OSC layer in the transistor channel (between source and drain electrodes) (Figure 1). The transistor efficiency is directly related to the channel dimensions (Figure 2) [19].
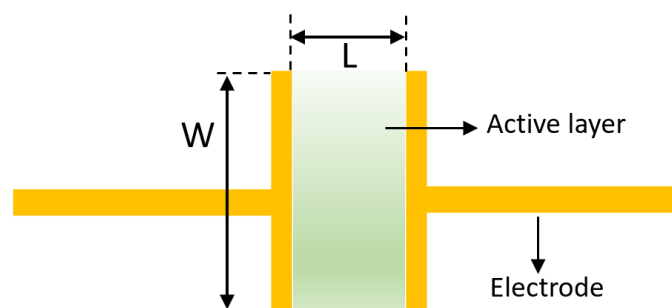

Figure 2. Scheme of source and drain electrodes forming channel with dimensions: W—width; L—length.

The maximum electrical current (I_{SD}) that can flow between source-drain (in a saturation regime) can be calculated from the following equation [16]:

$$I_{SD} = \frac{W}{2L} \mu C (V_G - V_T)^2 \qquad (1)$$

where W—channel width; L—channel length; C—capacitance of the dielectric; μ—charge carrier mobility of OSC material; V_G—voltage applied to the gate electrode; V_T—threshold voltage of the transistor.

According to Equation (1), the main factor determining the transistor efficiency, besides OSC and the dielectric materials, is the channel geometry. To ensure high efficiency of the device, the channel length ranges usually from few micrometers up to tens of micrometers [19,20]. Fast and economically viable fabrication of a customizable small channel with a precisely defined shape is a significant

engineering challenge. The technology of laser cutting of channels meets the above requirements. An important aspect is the edge of the mask, which should be cut in a straight line to obtain well-defined dimensions of the transistor channel. The channel dimensions directly influence the electrical current (I_{SD}) that can flow between source and drain electrode (Equation (1)) [19].

One of the electrode deposition methods used in organic electronics is vacuum thermal evaporation (vacuum 1×10^{-5} mBar). This method allows for precise application of electrodes by deposition of metal from vapor phase onto the sample in "high" vacuum through the so-called shadow mask or micro stencil. This mask is usually made of metal with apertures cut in the places, where the metal needs to be deposited through the mask onto the sample [21]. Electrodes obtained in the vacuum deposition process ideally reflect the dimensions and shape of the shadow mask (in negative). Shadow masks are used widely in nanotechnology for fabrication of majority of modern electronics such as processors or solid-state memory devices (SSDs). Such masks enable not only thermal vacuum deposition but also various sputtering, lithography, and electroforming processes in industries where high precision is of high importance. One of the challenges in production of shadow masks for micro- and nano-industries are the time-consuming and expensive processes such as UV-lithography, thus making rapid prototyping and customization of shadow masks difficult [22]. The proposed method is competitive with those used thus far due to the ease of adjusting the process parameters, time, and process ecology.

2. Materials and Methods

2.1. Laser Process

The masks were produced using a stand equipped with SPI G3.1 fiber laser (SPI Lasers UK Ltd., Southampton, UK), BET expander (SPI Lasers UK Ltd., Southampton, UK) with nominal magnification 8.7, Nutfield 3xB scanner (Thorlabs Inc., Newton, NJ, USA), telecentric lens (Thorlabs Inc., Newton, NJ, USA), and a self-focusing system with a distance sensor. The diagram of the stand is shown in Figure 3. The laser parameters are set using the driver from the WaveRunner application. In this way, the duration of the pulses, pulse repetition frequency, beam scanning speed, and beam power are regulated. From the laser, the beam is directed through the optical fiber to the expander, whose role is to collimate and extend the beam to a diameter of 9.1 mm. The shaped laser beam goes to the scanning device equipped with a two-axis galvanometric head. This solution gives the possibility of obtaining very high beam scanning speeds up to 6000 mm/s. The laser beam is focused to a spot with a diameter of 26 μm with the optical elements (expander, F-Theta lens). The positioning of samples is possible thanks to the precise XYZ stage with the SICK OD2-P85W20A2 distance sensor, which measures with an accuracy of 1 μm. Detailed parameters of individual elements of the system are presented in Table 1.
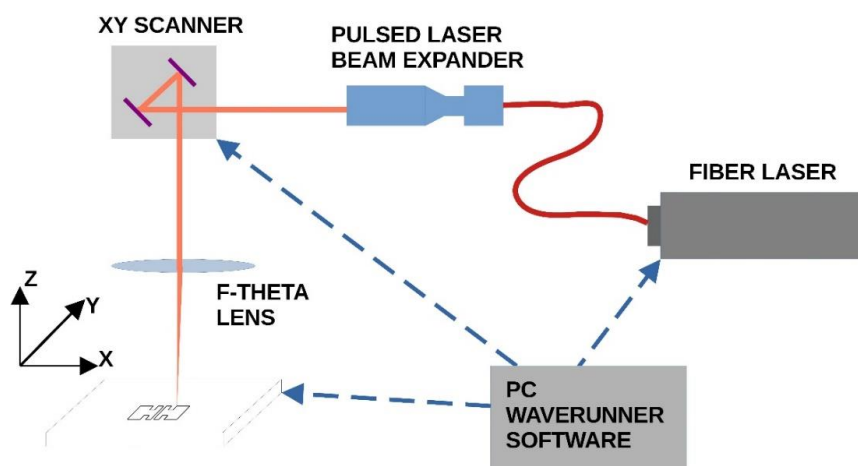

Figure 3. Diagram of the laser mask cutting system.

Table 1. Parameters of the devices of the laser system.

Laser SPI G3.1 SM 20 W	
Wavelength (nm)	1062
Average power (W)	20
Pulse duration (ns)	15–220
Pulse energy (mJ)	≤ 0.55
Frequency of repetition (kHz)	35–290
Quality of beam (M^2)	<1.3
Scanner (Nutfield Techn. Inc.)	
F-theta lens (mm)	100–164
Maximum scanning speed (mm/s)	6000
Pulsed Laser Beam Expander	
Mechanical Outline	7.0×8.7

Three types of ultra-thin films were used to produce the masks:

- Stainless steel SMT stencil foils PhD, 120 μm thick;
- Cold-rolled stainless, spring steel-1.4310, 35 μm thick;
- Hardened steel 1.1274, 30 μm thick.

2.2. Optimalization of the Mask-Cutting Process

For the tests, a number of test structures were produced in the form of two 1×1 mm openings with a bar in the center (Figure 4). The channel length was changed in the range of 50 to 300 μm.

The criteria for assessing the obtained elements were the following: the accuracy of mapping the dimensions of the bar, the continuity of the structure (the bar cannot be broken), and the smoothness of the cut edges.
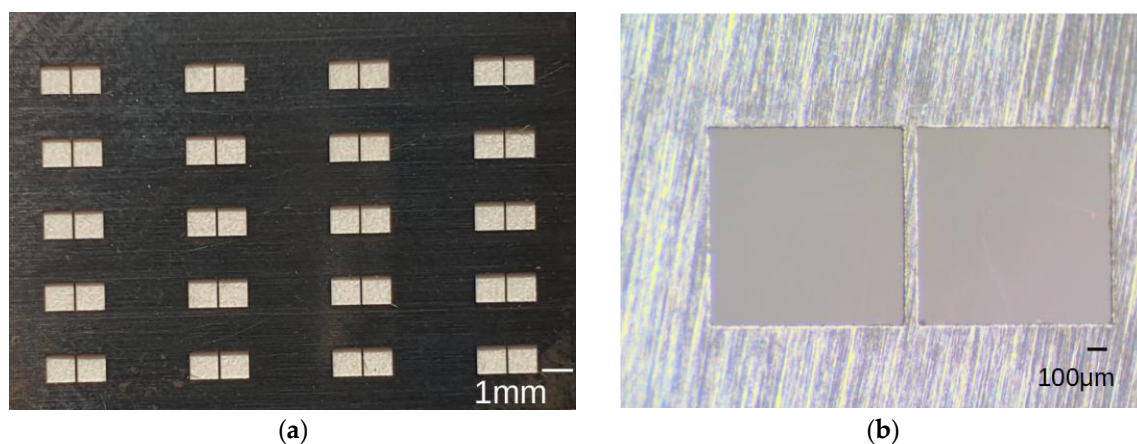

(**a**)　　　　　　　　　　　　　(**b**)

Figure 4. Microscopic photos of test structures—70 μm wide bar—hardened steel 1.1274, 30 μm: (**a**) magnification 5×; (**b**), magnification ×300.

The optimization of the parameters of the laser cutting process was performed using the experiment planning method [23,24]. The following parameters were set as the input parameters: laser beam power (2–10 W), pulse repetition frequency (35–270 kHz), beam speed (200–2000 mm/s), and pulse duration (15–220 ns). The starting factor was the thickness of the removed metal layer with a single exposure to the laser beam. A four-variable design with two levels of variation including interactions

was adopted to the research. The plan took into account the interaction between the beam scanning speed and the pulse repetition frequency due to the overlapping effect [25]. The most advantageous parameters were selected: pulse duration 25 ns, power 15 W, scanning speed 200 mm/s, and pulse repetition frequency 50 kHz. For these parameters, in order to cut holes in the foil of thickness of 35 μm and 30 μm, the scanning should be repeated 50 times. For a foil of thickness of 120 μm, pulses with a longer duration of 220 nm should be used. However, the bars obtained in these foils did not meet the assumed criteria and were not suitable to produce structures with dimensions below 70 μm.

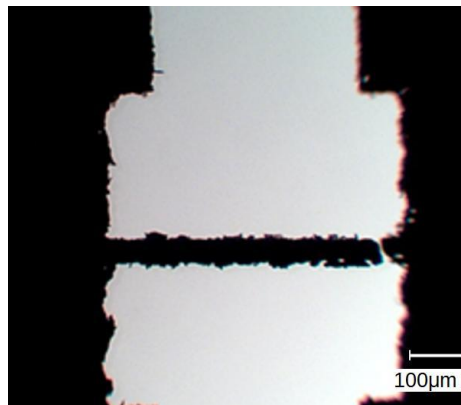Examples of incorrect structures with wrong selected parameters are shown in Figure 5.

Figure 5. A 50 μm thick mask with a broken channel; magnification ×100.

3. Results

In this work, we present a high-precision shadow masks for OFET (Figure 6) electrode evaporation fabricated by laser cutting. The photo shown in Figure 6 was taken with the Keyence Digital Microscope VHX-7000. The mask with overall dimensions of 85 × 75 mm included positioning holes and a set of 10 apertures grouped in 2 identical areas. The length of the channels in an individual mask varied from 100 to 300 μm. The masks were fabricated to make electrodes for flexible OFETs, which will be mechanically tested in the future. This range of channel length (100 to 300 μm) was chosen because such a long channel was the most suitable for our bending experimental setup.
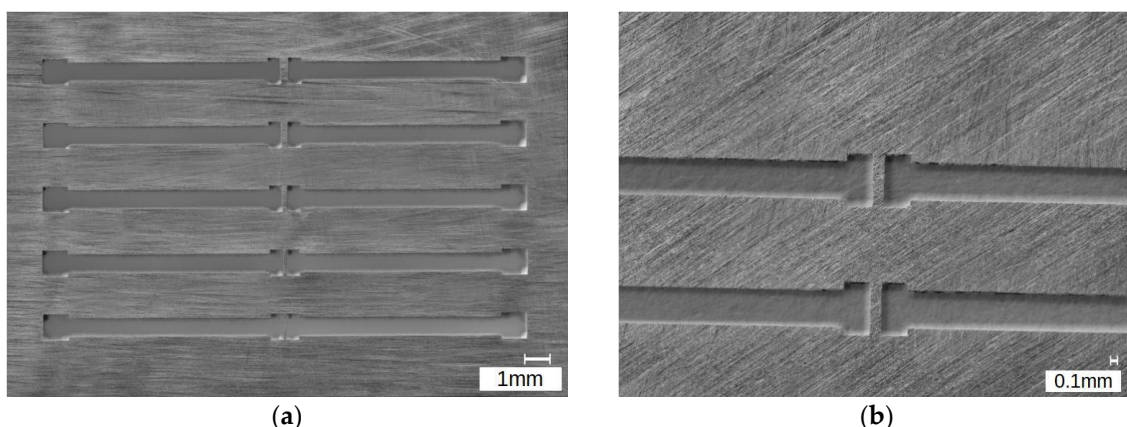

(**a**)   (**b**)

Figure 6. Shadow mask for organic field effect transistor (OFET) electrode fabrication with the channel lengths: 100, 150, 200, 250, and 300 (μm): (**a**) microscopic image (magnification ×10); (**b**) microscopic image channel length: 250 (μm), magnification ×30.

Electrodes obtained in the vacuum deposition process should ideally possess the same shape as the pattern of the mask. Therefore, an important aspect are the edges of the mask, which should be cut in a straight line to obtain well-defined dimensions of the transistor channel. Nevertheless, in practice,

the shape of electrode can be slightly different from the pattern of the mask (Figure 7a,b). This effect is related to the imperfections in the vacuum deposition process. The shape and the profile of an electrode depends on the angle at which the evaporated metal hits the sample (ideally it should be a right angle to reproduce the shape of the mask) as well as mask fitment to the surface of the sample to reduce overspray. In case of high roughness or uneven shape of the sample, the mask may not fit perfectly. Moreover, accumulated damage to the mask throughout its use and increasing thickness of metal deposited on the mask itself reduces the precision of produced electrodes. Because of this, it is important to replace the masks regularly. This increases cost and makes fast and cheaper mask production method more attractive [21,26]. The electrodes with thickness 100 nm were deposited through shadow mask (Figure 6) on the silicon/silicon-oxide (Si/SiO$_2$) wafer, coated with OSC. To ensure tight bonding of the mask to the surface of sample, the mask was pressed by special holder. The chosen evaporated metal was gold, because of the electrode work function providing suitable charge carrier injection from electrode to OSC during OFET operation.
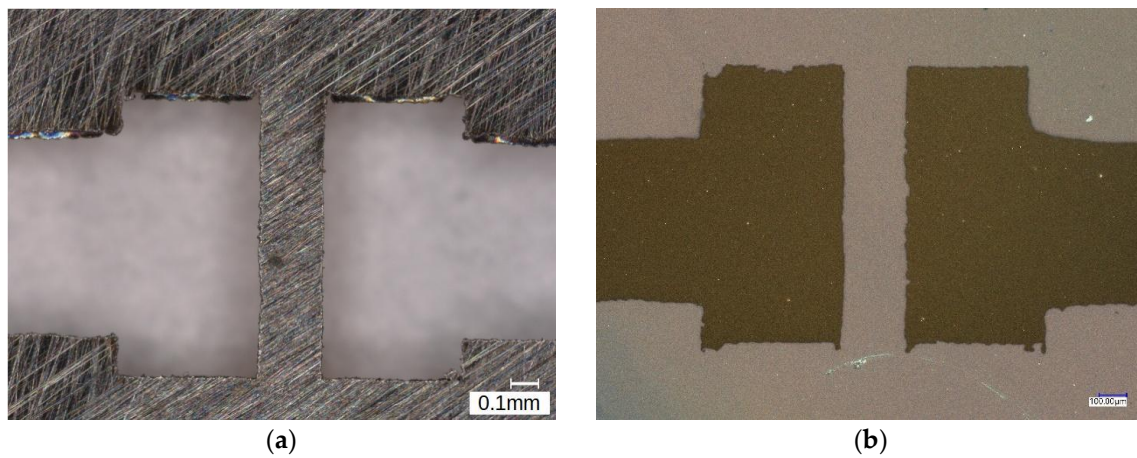

(**a**)　　　　　　　　　　　　　　　　　　　　　　　（**b**)

Figure 7. Microscope image of (**a**) shadow mask; (**b**) electrode obtained by vacuum evaporation of gold through shadow mask. The distance between electrodes is 250 μm, magnification ×150.

The functionality of electrodes was initially tested by using them as a source and drain electrodes in OFET devices with standard Si/SiO$_2$ wafers as substrates and using 2,7-dioctyl [1] benzothieno, [3,2-b] [1] benzothiophene (C8BTBT) as an OSC active layer. The C8BTBT is a high-performance p-type OSC that was deposited in a vacuum thermal deposition process. The transfer and output current–voltage characteristics (CVs) of the OFET are presented on the Figure 8.

The transistors were measured using a Keithley 2634B source meter. Output characteristics were measured with constant gate voltage (V$_{GS}$) ranging from 10 V to −60 V with step 10 V and variable drain–source voltage (V$_{DS}$) from 10 V to −60 V. Transfer characteristics were measured after applying constant drain–source voltage (V$_{DS}$) of −60 V and various gate voltages (V$_{GS}$) from 10 V to −60 V. The fabricated devices showed typical OFET current–voltage characteristics, with the following operational parameters: charge carrier mobility μ = 0.51 cm^{2}V^{-1}s^{-1}, threshold voltage V$_{th}$ = −21 V, and on/off current ratio I$_{on/off}$ = 8 × 10^4.

The mobility and threshold voltage of OFET were extracted from the saturation regime of the transfer characteristic using the following formula:

$$\mu = \frac{2L}{WC_i} \times \left(\frac{\partial \sqrt{I_{DS}}}{\partial V_{Gs}} \right)^2$$

where I$_{DS}$ is the source–drain current, V$_{GS}$ is the gate voltage, C$_i$ is the capacitance of gate dielectric layer, μ is the mobility in the saturation region, L is the channel length, and W is the channel width [19].
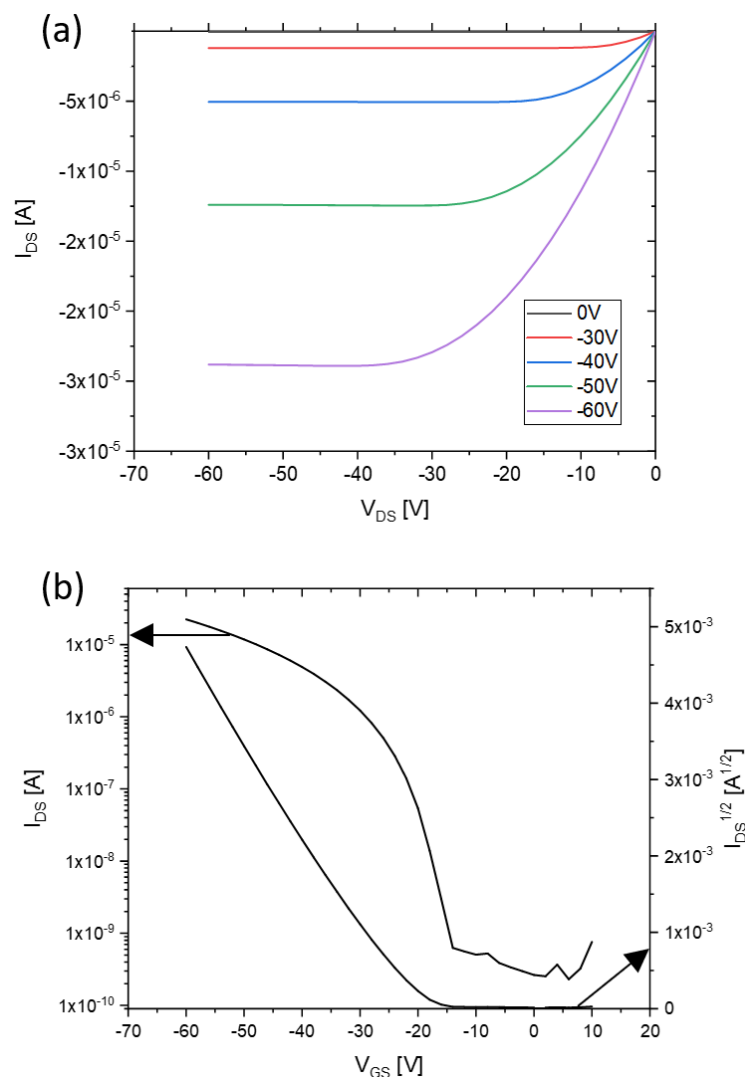
Figure 8. The (**a**) transfer and (**b**) output current–voltage characteristics of OFET fabricated with usage of source and drain golden electrodes, obtained by vacuum evaporation of gold through shadow mask. The OFET channel length of OFET was 250 µm and electrode configuration was bottom gate–top contact.

The operational parameters of the presented transistor are comparable to the literature values for C8BTBT semiconductor deposited on Si/SiO_2 wafer with gold electrodes [27,28]. This proves functionality of the source and drain electrodes deposited by masks obtained by laser ablation process.

4. Discussion

The use of a fiber laser with the described parameters makes it possible to produce masks with a canal with a minimum length of 70 µm. Masks prepared with narrower channels are not continuous, nor are the cut results with edges that are jagged. Irregularly shaped electrodes might present challenges to proper parameter calculation, increase overspray, and in more extreme cases cause short circuits or electrical arcing. This is the result of thermal stresses and deformations occurring when the thin foil heats up. Much better results were obtained for lower beam scanning speeds, which were related to the inertia of the scanning system. This effect cannot be observed in structures larger than 500 µm. Due to the impulse nature of laser interaction and the diameter of the focused beam (26 µm), the maximum edge smoothness was achieved with a layer thickness of up to 1 µm. However, it is an acceptable value in the technology of electrode evaporation in OFET transistors. The presented method offers facile and fast shadow mask fabrication for organic electronics application. While the minimum

dimensions of objects produced are limited in comparison to other methods, e.g., photolithography or electroforming, it is much cheaper because it does not require multi-step processes or high purity clean room conditions, and it uses commercially available materials. The presented method can be useful for fast prototyping and circuit design.

Author Contributions: Conceptualization, M.T., P.K.; data curation, M.T., P.K., W.W.; formal analysis, M.T., P.K., W.W.; investigation, M.T., P.K., W.W.; methodology, M.T., P.K., W.W.; supervision, M.T.; validation, M.T., P.K., W.W.; visualization, M.T., P.K., W.W.; writing—original draft, M.T., P.K., W.W.; writing—review and editing, M.T., P.K., W.W.; All authors have read and agreed to the published version of the manuscript.

Conflicts of Interest: The authors declare no conflict of interest.

References

1. Farson, F.; Feeley, D.F.T. (Eds.) *LIA Handbook of Laser Materials Processing*; Springer: Berlin/Heidelberg, Germany, 2001.
2. Steen, W.M.; Mazumder, J. *Laser Material Processing*, 4th ed.; Springer: London, UK; Dordrecht, The Netherlands; Heidelberg, Germany; New York, NY, USA, 2010.
3. Banat, D.; Ganguly, S.; Meco, S.; Harrison, P. Application of high power pulsed nanosecond fibre lasers in processing ultra-thin aluminium foils. *Opt. Lasers Eng.* **2020**, *129*, 106075. [CrossRef]
4. Korzeniewska, E.; Tomczyk, M.; Pietrzak, Ł.; Hadžiselimović, M.; Štumberger, B.; Sredenšek, K.; Seme, S. Efficiency of laser-shaped photovoltaic cells. *Energies* **2020**, *13*, 4747. [CrossRef]
5. Pawlak, R.; Tomczyk, M.; Walczak, M.; Sek, P.; Tanski, M. The efficiency and quality of silicon micromachining above the ablation threshold: A comparison for femto, pico and nanosecond laser. In Proceedings of the SPIE—The International Society for Optical Engineering, Jastarnia, Poland, 24–28 September 2018; Volume 10974, p. 109740X.
6. Pawlak, R.; Tomczyk, M.; Walczak, M.; Domagalski, P. Semiconductor and ceramic microstructure made by single mode fiber laser. *J. Phys. Conf. Ser.* **2014**, *494*, 012015. [CrossRef]
7. Siciński, M.; Korzeniewska, E.; Tomczyk, M.; Pawlak, R.; Bieliński, D.; Gozdek, T.; Kaluzinska, K.; Walczak, M. Laser-textured rubbers with carbon nanotube fillers. *Polymers* **2018**, *10*, 1091.
8. Ahmadivand, A.; Gerislioglu, B.; Ramezani, Z. *Toroidal Metamaterials: Fundamentals, Devices, and Applications*; Springer Nature: Berlin/Heidelberg, Germany, 2020.
9. Ahmadivand, A.; Gerislioglu, B.; Ahuja, R.; Mishra, A.K. Toroidal metaphotonics and metadevices. *Laser Photon. Rev.* **2020**, *14*, 1900326. [CrossRef]
10. Ahmadivand, A.; Semmlinger, M.; Dong, L.; Gerislioglu, B.; Nordlander, P.; Halas, N.J. Toroidal dipole-enhanced third harmonic generation of deep ultraviolet light using plasmonic meta-atoms. *Nano Lett.* **2019**, *19*, 605–611.
11. Pawlowski, S.; Plewako, J.; Korzeniewska, E. Analysis of flow field distribution in a thin conductive layer with an elliptical defect. *Przegląd Elektrotechniczy* **2020**, *96*, 234–237.
12. Servaites, J.D.; Ratner, M.A.; Marks, T.J. Organic solar cells: A new look at traditional models. *Energy Environ. Sci.* **2011**, *4*, 4410–4422. [CrossRef]
13. Someya, T.; Bauer, S.; Kaltenbrunner, M. Imperceptible organic electronics. *MRS Bull.* **2017**, *42*, 124–130. [CrossRef]
14. Nawrocki, R.A.; Matsuhisa, N.; Yokota, T.; Someya, T. 300-nm Imperceptible, Ultraflexible, and Biocompatible e-Skin Fit with Tactile Sensors and Organic Transistors. *Adv. Electron. Mater.* **2016**, *2*, 2–5. [CrossRef]
15. Bardagot, O.; Kubik, P.; Marszalek, T.; Veyre, P.; Medjahed, A.A.; Sandroni, M.; Grévin, B.; Pouget, S.; Domschke, T.N.; Carella, A.; et al. Impact of Morphology on Charge Carrier Transport and Thermoelectric Properties of N-Type FBDOPV-Based Polymers. *Adv. Funct. Mater.* **2020**, *30*, 1–11. [CrossRef]
16. TSekitani, T.; Zschieschang, U.; Klauk, H.; Someya, T. Flexible organic transistors and circuits with extreme bending stability. *Nat. Mater.* **2010**, *9*, 1015–1022. [CrossRef] [PubMed]
17. Zhang, L.; Wang, H.; Zhao, Y.; Guo, Y.; Hu, W.; Yu, G.; Liu, Y. Substrate-Free Ultra-Flexible Organic Field-Effect Transistors and Five-Stage Ring Oscillators. *Adv. Mater.* **2013**, *25*, 5455–5460. [CrossRef] [PubMed]

18. Ren, H.; Tang, Q.; Tong, Y.; Liu, Y. 320-nm Flexible Solution-Processed 2,7-dioctyl[1] benzothieno[3,2-b] benzothiophene Transistors. *Materials* **2017**, *10*, 918. [CrossRef]

19. Choi, H.H.; Cho, K.; Frisbie, C.D.; Sirringhaus, H.; Podzorov, V. Critical assessment of charge mobility extraction in FETs. *Nat. Mater.* **2018**, *17*, 2–7. [CrossRef]

20. Horowitz, G. Organic thin film transistors: From theory to real devices. *J. Mater. Res.* **2004**, *19*, 1946–1962. [CrossRef]

21. Zhou, Y.X.; Johnson, A.T.; Hone, J.; Smith, W.F. Simple Fabrication of Molecular Circuits by Shadow Mask Evaporation. *Nano Lett.* **2003**, *3*, 1371–1374. [CrossRef]

22. Naulleau, P. *Optical Lithography*; Elsevier Ltd.: Amsterdam, The Netherlands, 2019; Volume 1–5.

23. Korzeniewska, E.; Tomczyk, M.; Walczak, M. The influence of laser modification on a composite substrate and the resistance of thin layers created using the PVD process. *Sensors* **2020**, *20*, 1920. [CrossRef]

24. Pramanik, D.; Goswami, S.; Kuar, A.; Sarkar, S.; Mitra, S. A Parametric Study of Kerf Deviation in Fiber Laser Micro Cutting on Ti6Al4V Superalloy. *Mater. Today Proc.* **2019**, *18*, 3348–3356.

25. QLin, Q.; Fan, Z.; Wang, W.; Yan, Z.; Zheng, Q.; Mei, X. The effect of spot overlap ratio on femtosecond laser planarization processing of SiC ceramics. *Opt. Laser Technol.* **2020**, *129*, 106270.

26. Decker, W.; Belan, R.; Heydemann, V.; Armstrong, S.; Fisher, T. Novel low pressure sputtering source and improved vacuum deposition of small patterned features using precision shadow masks. In Proceedings of the Society of Vacuum Coaters 59th Annual Technical Conference, Indianapolis, IN, USA, 9–13 May 2016; Volume 1, pp. 556–571. [CrossRef]

27. Ablat, A.; Kyndiah, A.; Houin, G.; Alic, T.Y.; Hirsch, L.; Abbas, M. Role of Oxide/Metal Bilayer Electrodes in Solution Processed Organic Field Effect Transistors. *Sci. Rep.* **2019**, *9*, 6685.

28. Lee, J.H.; Kim, S.; Kim, H.; Lee, J. Solvent-dependent performance of solution-processed small-molecule organic field-effect transistors. *Org. Electron.* **2018**, *52*, 184–189. [CrossRef]

Publisher's Note: MDPI stays neutral with regard to jurisdictional claims in published maps and institutional affiliations.